ENGINEERING

Organic neuromorphic electronics for sensorimotor integration and learning in robotics

Imke Krauhausen[1,2], Dimitrios A. Koutsouras[1], Armantas Melianas[3,4], Scott T. Keene[5], Katharina Lieberth[1], Hadrien Ledanseur[1], Rajendar Sheelamanthula[6], Alexander Giovannitti[3], Fabrizio Torricelli[7], Iain Mcculloch[6,8], Paul W. M. Blom[1], Alberto Salleo[3]*, Yoeri van de Burgt[2]*, Paschalis Gkoupidenis[1]*

In living organisms, sensory and motor processes are distributed, locally merged, and capable of forming dynamic sensorimotor associations. We introduce a simple and efficient organic neuromorphic circuit for local sensorimotor merging and processing on a robot that is placed in a maze. While the robot is exposed to external environmental stimuli, visuomotor associations are formed on the adaptable neuromorphic circuit. With this on-chip sensorimotor integration, the robot learns to follow a path to the exit of a maze, while being guided by visually indicated paths. The ease of processability of organic neuromorphic electronics and their unconventional form factors, in combination with education-purpose robotics, showcase a promising approach of an affordable, versatile, and readily accessible platform for exploring, designing, and evaluating behavioral intelligence through decentralized sensorimotor integration.

INTRODUCTION

In all living organisms, the sensory and motor systems coordinate with each other, forming a unified entity (*1*–*4*). In this sensorimotor integration, the processing of senses in the sensory system occurs jointly with motor behaviors while, simultaneously, motor actions are under continuous sensory guidance. For instance, the action-to-sense direction can occur in vision (move of the body or saccadic eye movements to actively visualize the environment) and in olfaction (active sampling with sniffs to perceive a smell) (*5*). In the opposite direction of sense to action, sensory stimuli trigger motor actions, e.g., the presence of an object in the visual field initiates and guides movement (*6*). Even simple invertebrate organisms such as insects (e.g., drosophila, locust, etc.), whose neuronal circuits are easily traceable, exhibit a repertoire of intelligent behaviors due to sensorimotor integration (*7*). These behaviors are either hardwired and predefined (reflex-like) or learned as sensorimotor associations that are context dependent. More complex behaviors and learning build upon low-level reflexes and sensorimotor associations. A simplified mechanistic yet insightful version of sensorimotor integration was proposed by Braitenberg (*8*), with vehicles as a metaphor. In these hypothetical vehicles, primitive forms of intelligence that are found in low-level species such as exploratory, avoidance, and escape behavior emerge by coupling sensory signals and motor commands via excitatory/inhibitory and ipsilateral/contralateral connections (*8*–*12*). On top of this hardwired coupling, behavioral learning is promoted by adaptable sensory-to-motor connections, thus forming sensorimotor associations that represent a simple and generalized mechanism for behavioral emergence. Although conceptually primitive, these vehicles represent a prominent platform to develop and assess neuromorphic circuits for learning sensorimotor processes and behavioral tasks in robotics, as well as for energy-efficient and distributed data handling/processing (*13*–*15*).

Neuronal computation can be directly emulated in the analog-digital domain on neuromorphic circuits, thereby providing real-time communication between the analog world, accessed by the sensorimotor system and the digital unit(s) of robotic platforms (*13*, *16*–*18*). Nevertheless, these neuromorphic circuits are usually large scale and implemented in custom-made robotic systems (*13*, *16*–*19*). For example, the silicon-based SpiNNaker engine, which has been used for sensorimotor learning, consists of 48 chips and 18 processors per chip (*16*, *17*). Despite the notable demonstrations of high complexity, an in materio computing perspective may provide elegant and simplified solutions in robotics. Emerging materials and devices, for instance, have novel properties and can unlock circuit functionalities unattainable by conventional electronics, as they are able to emulate directly bioinspired and biorelevant functionalities such as synaptic plasticity, neuronal functions, homeostasis, and self-healing ability, without needing complex circuitry (*20*). Moreover, the mechanics of the embodiment (i.e., physical body) are crucial in robotics, for instance, the use of inertia for energy-efficient locomotion and morphological adaptation for locomotion in unstructured or complex environments (*19*, *21*, *22*). Small-scale (i.e., simple and consisting of limited components) neuromorphic circuits for sensorimotor control and optimization of the utmost simplicity are thus of great importance for understanding the fundamental relationships between the sensory and motor systems. Only recently, small-scale neuromorphic circuits based on metal oxide neuromorphic devices have been used for local computation and control in robotic systems. Improved balance with low-latency and adaptive behavior in mobile robotics has been achieved with memristor-based adaptive filters and arrays (*23*, *24*). Robotic arm control that is tolerant to damages has also been demonstrated with metal oxide transistors (*25*). Nevertheless, in the above cases, learning is either offline (*23*) or outside the sensorimotor loop (*24*), and the implementation requires many conventional silicon components (*23*–*25*).

[1]Max Planck Institute for Polymer Research, Mainz, Germany. [2]Microsystems, Institute for Complex Molecular Systems, Eindhoven University of Technology, Eindhoven, Netherlands. [3]Department of Materials Science and Engineering, Stanford University, Stanford, CA 94305, USA. [4]Exponent, 149 Commonwealth Dr, Menlo Park, CA 94025, USA. [5]Department of Engineering, University of Cambridge, Cambridge, UK. [6]KAUST Solar Center, Physical Science and Engineering Division, King Abdullah University of Science and Technology (KAUST), Thuwal, Saudi Arabia. [7]Department of Information Engineering, University of Brescia, 25123 Brescia, Italy. [8]Department of Chemistry, University of Oxford, Oxford, UK.
*Corresponding author. Email: asalleo@stanford.edu (A.S.); y.b.v.d.burgt@tue.nl (Y.v.d.B); gkoupidenis@mpip-mainz.mpg.de (P.G.)

Organic electronic materials have recently emerged for neuromorphic electronics because of excellent tuneability, high stability, and low-voltage, low-power operation (*26*–*31*). Organic materials are soft, can be solution-processed or printed at relatively low thermal budget, and can be integrated on large-area, rigid, as well as conformal substrates (*32*, *33*). The flexible and biocompatible nature and the mixed ion-electronic conduction of semiconducting polymers also allow for enhanced connections with biological and biohybrid systems (*34*, *35*). Despite these notable demonstrations, organic neuromorphic circuits have only been assessed so far for their trainability and adaptability in on-bench applications such as small-scale artificial neural networks, logic gates, and sensors (*35*, *36*), all systems that perceive the external stimuli without any behavioral context and outcome. However, building and evaluating intelligent systems require a holistic approach with embodiment, with agents that perform actions to explore the environment and perceive in real time the corresponding consequences (*4*, *14*, *37*). Creating sensorimotor associations in locally trained organic neuromorphic circuits with ease of fabrication and unconventional form factors (i.e., solution processable, printable, large-area integration, and mechanical conformity) can lead to optimized systems with "on the edge" decentralized/distributed learning and reduced communication latencies (via large-area integration in flexible/stretchable substrates), fault tolerance due to redundancy or self-repairing (via large-area integration and self-healing ability), versatility, and low-power consumption (via low-voltage operation).

In this work, we introduce sensorimotor integration and local learning in a target behavioral task that requires mobility, which is enabled by a simple and low-voltage organic neuromorphic circuit. A standalone robot learns to navigate itself in a two-dimensional maze by following a planned path, after training its organic neuromorphic circuit with direct and real-time feedback from the sensorimotor system (Fig. 1A). Through online learning within the sensorimotor loop, the organic neuromorphic circuit establishes an

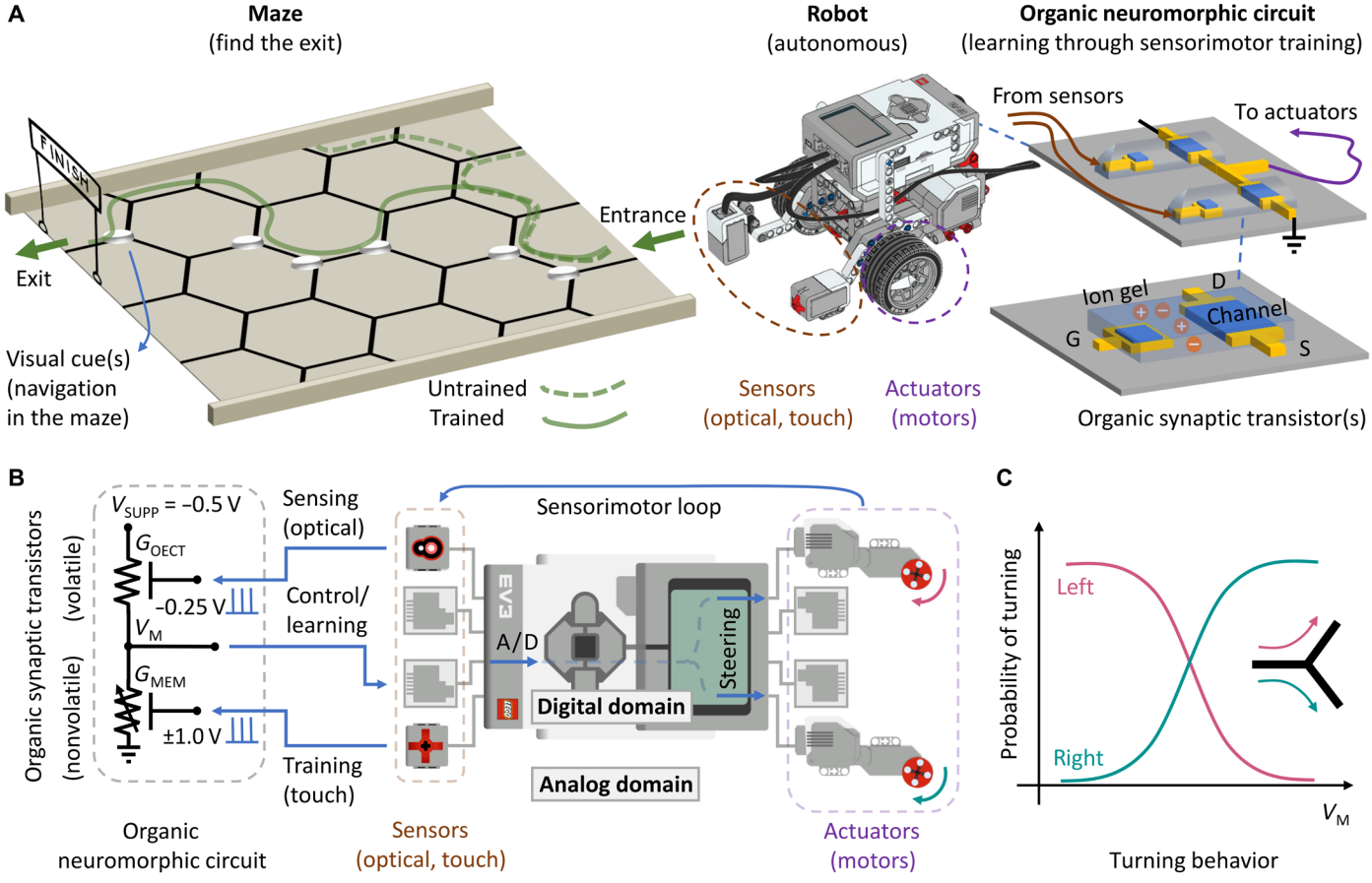

Fig. 1. Path-planning robot with an organic neuromorphic circuit for sensorimotor integration. (**A**) An autonomous robot gradually learns to navigate in a maze by following navigation cues to the exit. Processing and learning toward the target task are achieved locally with an organic neuromorphic circuit. (**B**) Detailed schematic of the robotic system. Static, low-level control of the sensorimotor system is carried out by a central unit in the digital domain. The sensorimotor system and the organic neuromorphic circuit operate in the analog domain, and a real-time, sensorimotor loop is established between the control unit (digital domain) and the sensorimotor system/neuromorphic circuit (analog domain). The neuromorphic circuit consists of organic synaptic transistors: a volatile (OECT) and a nonvolatile (MEM) device. While operating within the loop, the neuromorphic circuit receives optomechanical sensory signals (at the gates of the devices G_{OECT} and G_{MEM}) to perceive (adapt) the (to the) environmental stimuli and sends motor commands (V_M) to the actuators of the robot for locomotion. With its trainability and adaptivity, the circuit forms sensorimotor associations through training that are necessary for accomplishing the target task. (**C**) The turning behavior of the robot at a maze intersection is influenced nondeterministically and in real time by the output voltage V_M of the neuromorphic circuit.

association between the robot's sensory and motor units. This association is necessary for accomplishing the navigation task. Specific motor actions are triggered by visual stimuli that function as navigation cues. This sensorimotor integration, which happens locally and in the analog domain, guides the robot to the exit. The robot, its sensors/actuators, and the neuromorphic circuit are battery-powered and operate autonomously. The work showcases the use of organic neuromorphic electronics as local and decentralized learning circuitry for mobile applications in environments with energy restrictions.

RESULTS

The robotic system consists of two parts: the sensorimotor system along with organic neuromorphic circuit that operates in the analog domain and the robotic controller in the digital domain (Fig. 1B and fig. S1); both systems operate autonomously and locally on the robot. The robotic system senses the environment by collecting optical and mechanical signals with its reflectance and touch sensors, while locomoting in the quasi–two-dimensional maze with its two, left and right, servomotors. The maze consists of black-lined, hexagonal unit cells arranged in a honeycomb-like pattern. The digital control unit of the robot, a LEGO MINDSTORMS EV3 brick (*38*), optically traces the lined maze by means of reflectance and forwards actuation commands to the motors. The digital unit is controlled by a static, low-level line follower algorithm (i.e., stereotyped, reflex-like behavioral response), which ensures that the robot stays on the straight tracks of the maze between the intersections. Motor commands are continuously driven by optomechanical sensory signals (i.e., from the reflectance and touch sensors), while, simultaneously, motor actions modulate the sensory processes. A real-time sensorimotor loop is therefore formed. An analog and trainable neuromorphic circuit intervenes locally within the loop and provides learning through adaptive sensorimotor associations. The neuromorphic circuit consists of a nonvolatile and a volatile organic synaptic transistor [indicated as MEM (memory) and OECT (organic electrochemical transistor) devices, respectively; Fig. 1B], which are connected in series and, in essence, form a trainable voltage divider. The output voltage V_M depends on the resistance ratio between the two synaptic devices, as well as on their sensory input signals.

The algorithm of the digital unit is static and thus creates a fixed behavioral frame when the robot approaches a maze intersection. The algorithm alone has no agency on the actual direction of turning but can favor left or right steering depending on its input variable(s) that temporally modifies the motor power distribution (section S1 and fig. S2). The input variable(s) is provided by the organic neuromorphic circuit in real time, as analog voltage V_M. V_M is then digitized with a 12-bit-resolution analog-to-digital converter to be handled by the algorithm that is executed at the control unit. While providing the output voltage V_M to the control unit, the neuromorphic circuit receives optical sensory signal from the reflectance sensor at the gate G_{OECT} and mechanical sensory signal from the touch sensor at the gate G_{MEM}. The reflectance signal is used for sensing the maze track, and the mechanical signal of the touch sensor represents the environmental stimulus for reinforced learning. The sensory signals are conditioned and downscaled by an additional analog hardware unit to match with the low-operation voltages of the synaptic devices ($\leq$0.5 V; section S2 and figs. S1 and S3).

As the robot follows a straight line in the maze and approaches an intersection, the actual turn outcome depends on the instantaneous power distribution between the left and right motors. This instantaneous distribution is temporarily driven by the output voltage V_M of the organic neuromorphic circuit, as it receives the optomechanical sensory inputs. Because of the oscillatory-like scanning of the maze track with the robot by means of the line follower algorithm (fig. S2), the steering direction in an intersection is nondeterministic with probability that depends on the voltage V_M (Fig. 1C).

The organic neuromorphic circuit is made of 2-μm-scale synaptic devices based on OECTs (Fig. 2A and fig. S4). The channel material of the transistors, an organic mixed ionic-electronic conductor, is gated via an electrolyte, and an ionic gate current can modulate the electronic current that flows through the channel (*34*, *39*). Both devices are fabricated using the solution-processed polymer poly(2-(3,3′-bis(2-(2-(2-methoxyethoxy)ethoxy)ethoxy)-[2,2′-bithiophen]-5-yl) thieno [3,2-b] thiophene) [p(g2T-TT)] as a channel material. An ionic gel [1-ethyl-3-methylimidazolium bis(trifluoromethylsulfonyl)imide (EMIM:TFSI) with polyvinylidene fluoride-co-hexafluoropropylene (PVDF-HFP)] between the channel and the gate serves as the electrolyte of the device (*40*). p(g2T-TT) exhibits mixed conduction, as it is an organic hole-transporting semiconductor and also an ion-conducting material. p(g2T-TT) has been chosen as a channel material in both volatile and synaptic electrochemical transistors as it yields properties that are necessary for the device elements of the neuromorphic circuit, such as a wide dynamic range of resistance tuning (~100× analog memory window), high transconductance (~μS to mS), and endurance (~10^8 write-read events) at low-voltage operation ($|V| < 0.5$ V) (*30*, *41*). The differentiation between volatility and nonvolatility depends on the probing conditions of the devices. Nonvolatility is induced by enforcing gate-to-channel open-circuit potential condition via an analog switch (i.e., the touch sensor), while probing the gate electrode directly incites volatile behavior (*29*, *30*). Therefore, monolithic integration of both transistor functionalities (volatile/nonvolatile) with the same channel and electrolyte materials is achievable for the implementation of the organic neuromorphic circuit, thus notably simplifying the fabrication process and material selection (fig. S4).

The volatile synaptic part of the trainable neuromorphic circuit resembles an OECT. Transistor characteristics that demonstrate reliable switching behavior at ultralow operation voltages are obtained (Fig. 2B and fig. S5). For instance, in the OECT-only case, operation voltages of the transfer (I_D versus $V_{G,OECT}$) and output (I_D versus $V_{D,OECT}$) characteristics are <0.4 V, with I_D as the drain current and $V_{G,OECT}$ and $V_{D,OECT}$ as the gate and drain voltage, respectively. The transconductance $g_{m,OECT}$ ($=dI_D/dV_{G,OECT}$), which defines the efficiency of the device to amplify a sensory input signal ($V_{G,OECT}$) at the output (I_D), depends monotonically on the drain voltage $V_{D,OECT}$ (section S3). By connecting a variable load resistor R_{MEM} in series to the OECT in a voltage divider topology, the voltage partition V_M (or equivalently $V_{D,OECT}$) and thus $g_{m,OECT}$ depend on the ratio of the OECT to load resistance, R_{OECT}/R_{MEM} (Fig. 2C and section S3). A ratio in the range of R_{OECT}/R_{MEM} = 1 to 100 is sufficient to modify V_M from $V_{SUPP}/2$ to 0 V and to amplify or even completely suppress a $V_{G,OECT}$ signal (in Fig. 2C shown as $g_{m,OECT}$). In the time domain response of the circuit (inset of Fig. 2C), R_{OECT}/R_{MEM} defines both the baseline V_M level (no sensory input signal; $V_{G,OECT} = 0$) and its amplification (for a sensory perturbation; $V_{G,OECT}$). The response time of the neuromorphic circuit is compatible with the oscillatory scanning of the maze track (fig. S6).

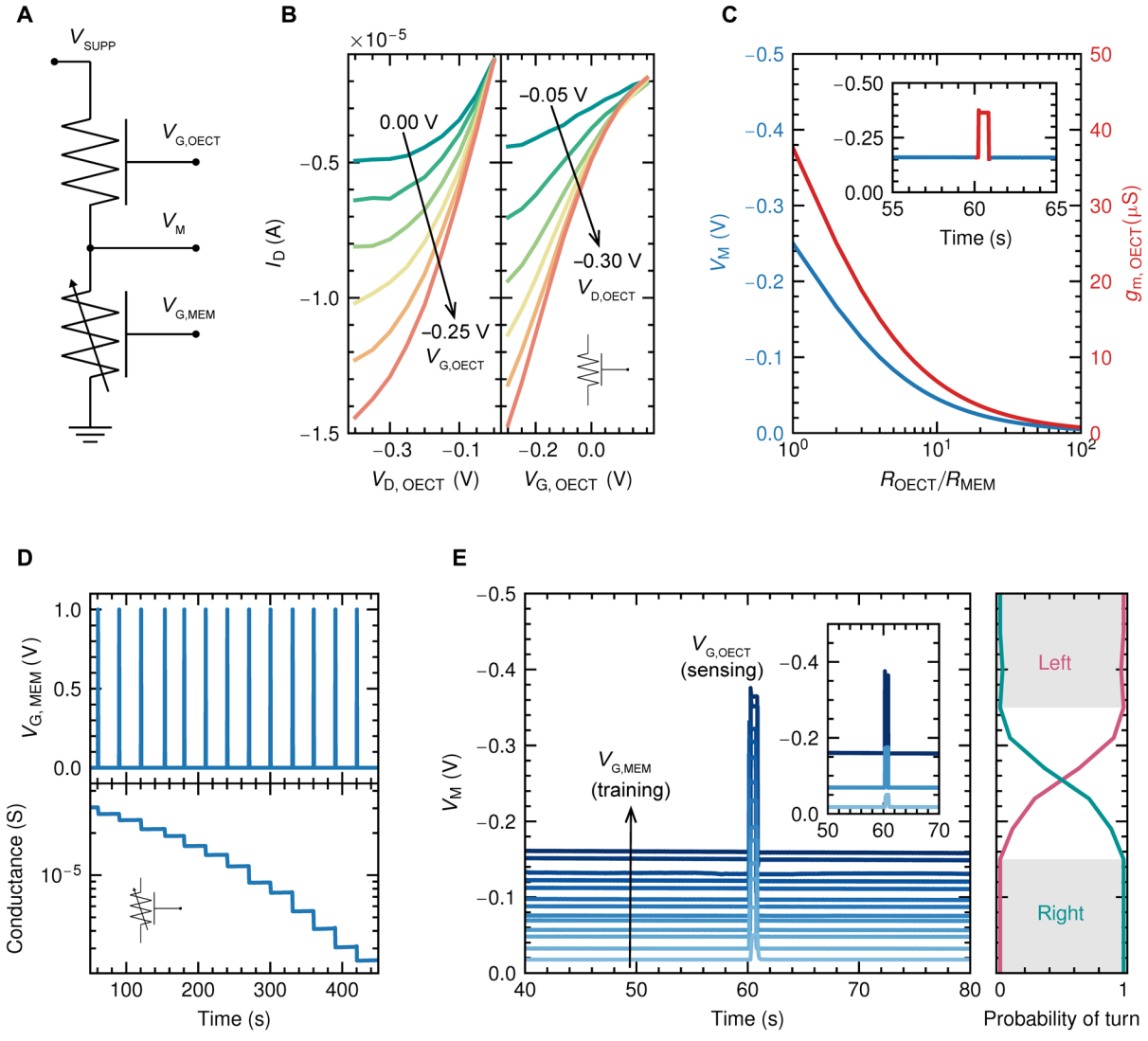

Fig. 2. Organic neuromorphic circuit for adaptive sensorimotor processing and control. (**A**) The organic neuromorphic circuit consists an OECT and an organic artificial synapse (MEM), forming a trainable/adaptive voltage divider (V_{SUPP} = −0.5 V). (**B**) Transfer (I_D versus $V_{G,OECT}$) and output (I_D versus $V_{D,OECT}$) characteristics of the transistors. (**C**) Calculated output voltage V_M of the organic neuromorphic circuit and OECT transconductance $g_{m,OECT}$ as a function of the OECT-to-MEM resistance ratio, R_{OECT}/R_{MEM}. A ratio R_{OECT}/R_{MEM}~100 is necessary to modulate V_M from 0 to $V_{SUPP}/2$ (blue line) and suppress/enhance $g_{m,OECT}$ (red line). The change of ratio R_{OECT}/R_{MEM} affects the baseline of V_M (inset, blue) and the amplification of signals through $g_{m,OECT}$ (inset, red). The R_{MEM} is emulated with a variable load resistor. The device model and its parameters used for calculations are shown in section S3. (**D**) Adaptability of the organic artificial synapse (MEM). Conductance levels of the device channel for a series of mechanosensory voltage pulses $V_{G,MEM}$, applied at the gate electrode ($V_{G,MEM}$ = 1 V, t~1 s). A memory window of ~100× is achieved. The number of states and their spacing depends on the pulsing conditions. (**E**) Output voltage V_M of the organic neuromorphic circuit over time, as the circuit receives optomechanical sensory signals; $V_{G,OECT}$, optical tracking of the maze ($V_{G,OECT}$ = −0.25 V, for ≳20 ms); $V_{G,MEM}$, touch sensor for reinforced learning ($V_{G,MEM}$ = −1 V, for ~1 s). The turn behavior of the robot depends on the instantaneous state of V_M.

A trainable neuromorphic circuit is realized with an organic artificial synapse (MEM) that exhibits tunable and nonvolatile conductance states, according to the circuit topology displayed in Fig. 2A. The conductance of the synaptic device is modulated reversibly by a series of voltage pulses $V_{G,MEM}$ at the gate electrode through an analog switch (i.e., the touch sensor). The synaptic device exhibits a high-memory window of >100× and stable, multiple memory states (Fig. 2D and fig. S7). The memory window of the synaptic device is sufficient to change the voltage partition V_M of the trainable voltage divider and therefore the OECT transconductance $g_{m,OECT}$. At the trainable circuit topology, the MEM gate receives training voltage pulses $V_{G,MEM}$ (1 V for ~1 s) that modulate the baseline level of V_M, and the OECT gate is biased with real-time sensory signal $V_{G,OECT}$ (−0.25 V for ≳20 ms) from the maze track (Fig. 2E). The characteristics of the neuromorphic circuit are accurately modeled in fig. S8. The neuromorphic circuit is simulated in static and transient conditions as a function of the sensory and training signals. The OECT exhibits a tunable sensitivity that depends on the resistance ratio of the two channels, R_{OECT}/R_{MEM} (at ~60 s; Fig. 2E). When $R_{OECT}/R_{MEM} \gg 1$, the baseline of the voltage

partition is V_M~0 V, and the OECT sensitivity for tracking the maze is minimum; through training, $R_{OECT} \approx R_{MEM}$, and the sensitivity increases significantly (fig. S9). V_M is digitized and forwarded to the control unit in real time as input for the static line follower algorithm. The static algorithm is executed by receiving dynamic input from V_M that depends on the external sensory signal stream. The dynamic input temporally modifies the motor power distribution and therefore the steering at a maze intersection. Depending on the V_M state, right ($|V_M| \leq 150$ mV) or left ($|V_M| \geq 350$ mV) steering is favored at an intersection, with a nondeterministic transitional region in between (sections S1 and S5 and fig. S10).

The navigation of the robot in the maze is achieved by gradually forming a visuomotor association between a visual cue and a motor action through training, which results in a behavioral outcome (visualized in a unit cell intersection at Fig. 3A). Before the training phase, visuomotor association is yet to be established. Although visual cues for navigation are present, the neuromorphic circuit is initialized in a way that its electric response toward the cues is low without inducing any behavioral outcome. The robot turns right at every intersection (V_M response in light blue; Fig. 2E). During training, the association is reinforced by an external mechanical stimulus (i.e., noxious stimulus or punishment) when the robot fails to execute the target behavior (i.e., when moving off the planned path toward the exit or falsely reaching the boundaries of the maze). The external stimulus is applied via the touch sensor (by an external trainer or when the robot hits the maze boundaries) at the MEM gate, G_{MEM}, while the robot is optically exploring the maze through the sensory signal of the OECT gate, G_{OECT}. With each training step, the behavioral adaptation is twofold: The baseline of V_M is moving upward in the probability curve of turning and the sensitivity toward navigation cues is enhanced (V_M response in medium blue; Fig. 2E). After training, the baseline of V_M still lies in the "turn right" regime of the probability curve. Nevertheless, $g_{m,OECT}$ is now increased significantly, and, in the presence of a navigation cue, V_M temporally shifts into the "turn left" regime (V_M response in dark blue; Fig. 2E). The visuomotor association is therefore formed, and visual cues trigger a behavioral outcome: no visual cue, right turn; presence of a visual cue, left turn. The planned path is marked by placing navigation

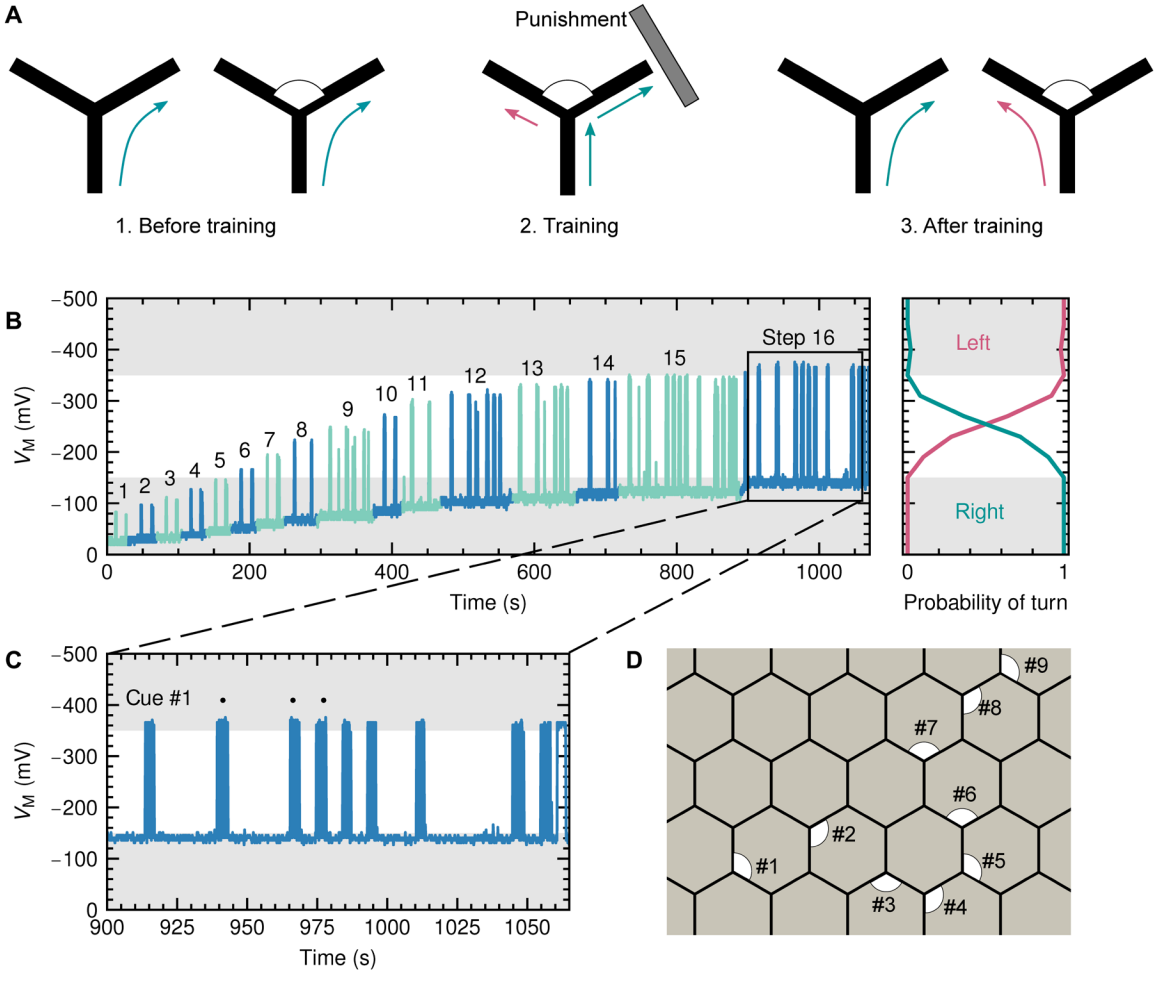

Fig. 3. Training process and formation of sensorimotor association. (**A**) Training process of the robot showing the formation of the visuomotor association. After training, the robot learns to associate navigation cues with motor actions, thus displaying a behavioral outcome. (**B**) Temporal evolution of the output voltage V_M during training, in respect to the probability curve of turning. Alternate colors in the V_M graph correspond to sequential training steps ($n = 1$ to 16 training steps). (**C**) V_M over time for the final training step, showing the detection of navigation cues that induces the temporal reversal of the turning probability. (**D**) Maze setup. The planned path is marked by navigation cues (#1 to #9) that indicate a left turn, otherwise a right turn.

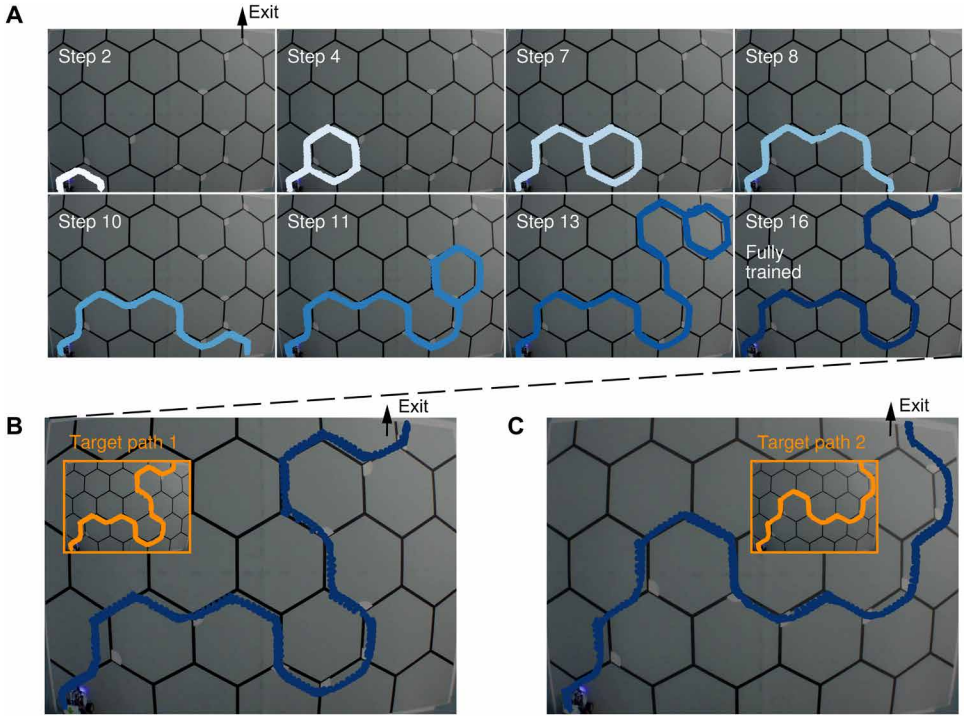

Fig. 4. Navigation in the maze toward the exit. (**A**) Training evolution inside the maze, visualized as path trajectories. After each training step (n = 1 to 16), the robot gradually learns to follow a target path through the navigation cues toward the exit of the maze. (**B**) Completion of target path 1 inside the maze, once the visuomotor association has been established (training step n = 16). (**C**) Generalization of the learning process in another, arbitrary path (example of target path 2). Photo Credit: Imke Krauhausen, Max Planck Institute for Polymer Research.

cues (circle arcs) in specific maze intersections that indicate a left turn, otherwise a right turn.

Figure 3B presents the temporal response of V_M throughout the whole training process in correlation with the probability curve of turning (n = 1 to 16 training steps). For the specific operation/training parameters used here (i.e., time and amplitude of $V_{G,OECT}$ and $V_{G,MEM}$), the robot is fully trained after ~16 steps (Fig. 3C) and thus is able to detect the navigation cues of the planned path (Fig. 3D). The evolution of the training process is depicted for the target path 1 (Fig. 4, A and B). The data are extracted by video tracking of the robot trajectory (section S4 and movie S1). The robot makes gradual progress in completing the target path in accordance with the temporal response of V_M (Fig. 3B). For n = 16, the robot is fully trained and exits the maze via the planned path. More detailed statistics of the training process is shown in fig. S11. After forming the visuomotor association, the robot is able to follow an entirely unknown path universally and exit the maze. In Fig. 4C, the robot is placed at the entrance of target path 2 and follows the newly planned path to the exit immediately. This generalization of learning through the sensorimotor association is shown in movie S2 in the case of navigation in target path 2.

DISCUSSION

Inspired by the biological process of sensorimotor integration, we demonstrated a standalone robot that learns with a simple yet effective neuromorphic circuit. An organic neuromorphic circuit is used as a low-voltage, analog computing core of the sensorimotor loop in robotics made of education-purpose components. While the robot explores the environment, real-time sensorimotor signals are merged in the organic neuromorphic circuit, and, through local/decentralized training on the circuit, a visuomotor association is gradually formed. With this sensorimotor integration, the robot learns to associate navigation cues with behavioral outcome and is able to follow a planned path to the exit of a maze. Once the sensorimotor association is established, the robot is able to navigate inside the maze toward the exit through unknown paths.

This demonstration shows how low-voltage and easy-to-tune organic devices can function as adaptive elements capable of forming multimodal associative links for autonomous learning. It highlights the ease of fabrication, integration, and training of organic neuromorphic circuits for decentralized sensorimotor integration and paves the way for sophisticated systems that include a plethora of sensory streams to allow more complex behaviors, advanced learning in circuits, or even in materio sensing, computing, and actuating with high-performing organic materials. By integrating sensory, actuating, learning, and self-repairing primitives in materio, intelligence can be distributed and incorporated in the fabric of agents. The combination of organic neuromorphic electronics with education-purpose robotics will also lead to a versatile platform for physical modeling and rapid prototyping of intelligent, real-world systems.

MATERIALS AND METHODS

Device fabrication

Standard microscope glass slides (75 mm by 25 mm) were cleaned in a sonicated bath, first in soap solution [Micro-90 (Sigma-Aldrich)] and then in a 1:1 (v/v) solvent mixture of acetone and isopropanol.

Gold electrodes for source, drain, and gates were photolithographically patterned [with positive MICROPOSIT S1813 Photoresist (Dow)] on the cleaned glass slides. A chromium layer was used to achieve better adhesion of the gold. Each glass slide contains four circuits consisting of one OECT and one neuromorphic device. The channel dimensions of the neuromorphic device are as follows: $W \times L = 80$ μm by 240 μm with a lateral gate of the same size (80 μm by 240 μm) and 450-μm distance between the gate and the channel. The OECT has the following dimensions: $W \times L = 80$ μm by 480 μm with a lateral gate of 2000 μm by 2000 μm and 450-μm distance between the gate and the channel. The complete layout is depicted in fig. S4A. Two layers of parylene C [Specialty Coating Systems (SCS) coatings] were deposited. Soap [Micro-90 soap solution, 1% (v/v) in deionized water] was used for separation between the layers, allowing the peel-off of the upper layer. An adhesion promoter [silane A-174 (γ-methacryloxypropyltrimethoxysilane) (Sigma-Aldrich)] was added to the lower layer of parylene C to prevent detachment. This layer insulates the gold electrodes. In a second photolithography step [with positive photoresist AZ 9260 Microchemicals (Cipec Spécialités)], the channel and lateral gate dimensions of the devices are defined. Reactive ion etching with O_2/CF_4 plasma was used to carve out the channel and corresponding gates. The semiconducting polymer p(g2T-TT) was synthesized according to (*41*) and prepared and applied following the procedure in (*30*, *41*). p(g2T-TT) was solved in chloroform (3 mg/ml) inside an N_2-filled glove box and spin-cast under ambient conditions at 1000 rpm for 1 min, resulting in a thickness of 40 nm. The devices were baked at 60°C for 1 min. The sacrificial upper parylene C was peeled off to confine the polymer inside the gate and channel regions. Excess soap was rinsed off with de-ionized water. An ionic gel was prepared as electrolyte according to (*40*). An ionic liquid EMIM:TFSI and the copolymer PVDF-HFP were solved in acetone inside an N_2-filled glove box in the following proportions: 17.6 weight % (wt %) ionic liquid, 4.4 wt % polymer, and 76 wt % acetone. The solution was stirred for at least 2 hours at 40°C inside the glove box. The ionic gel was drop-cast with a pipette onto each channel and gate under ambient conditions and dried overnight (fig. S4B).

Measurements

For measurements of the nonvolatile device (MEM), a Keithley 2604B SourceMeter was used. A switch (i.e., a binary-state touch sensor) in series with a resistance $R_G = 100$ MΩ was added between the gate of the device G_{MEM} and the measurement system to induce analog memory phenomena. The touch sensor forces open-circuit potential condition between the gate and channel, while the gate resistor R_G downscales and limits the gate current in the range of nanoamperes. The measurements of the volatile device (OECT) and the complete neuromorphic circuit were performed with a Keithley 4200 semiconductor characterization system with up to 5 source measure units.

SUPPLEMENTARY MATERIALS

Supplementary material for this article is available at https://science.org/doi/10.1126/sciadv.abl5068

REFERENCES AND NOTES

1. D. M. Wolpert, Z. Ghahramani, Computational principles of movement neuroscience. *Nat. Neurosci.* **3**, 1212–1217 (2000).
2. M. Flanders, What is the biological basis of sensorimotor integration? *Biol. Cybern.* **104**, 1–8 (2011).
3. D. M. Wolpert, Z. Ghahramani, M. I. Jordan, An internal model for sensorimotor integration. *Science* **269**, 1880–1882 (1995).
4. G. Buzsáki, *The Brain From Inside Out* (Oxford Univ. Press, 2021).
5. N. Uchida, A. Kepecs, Z. F. Mainen, Seeing at a glance, smelling in a whiff: Rapid forms of perceptual decision making. *Nat. Rev. Neurosci.* **7**, 485–491 (2006).
6. M. Glickstein, How are visual areas of the brain connected to motor areas for the sensory guidance of movement? *Trends Neurosci.* **23**, 613–617 (2000).
7. S. J. Huston, V. Jayaraman, Studying sensorimotor integration in insects. *Curr. Opin. Neurobiol.* **21**, 527–534 (2011).
8. V. Braitenberg, *Vehicles: Experiments in Synthetic Psychology* (MIT Press, 2004).
9. D. B. Dusenbery, *Living at Micro Scale: The Unexpected Physics of Being Small* (Harvard Univ. Press, 2011).
10. D. L. Gunn, R. B. Lindsay, *The Orientation of Animals: Kineses, Taxes and Compass Reactions* (Harvard Univ. Press, 1961).
11. B. Webb, Robots in invertebrate neuroscience. *Nature* **417**, 359–363 (2002).
12. D. Floreano, A. J. Ijspeert, S. Schaal, Robotics and neuroscience. *Curr. Biol.* **24**, R910–R920 (2014).
13. M. B. Milde, H. Blum, A. Dietmüller, D. Sumislawska, J. Conradt, G. Indiveri, Y. Sandamirskaya, Obstacle avoidance and target acquisition for robot navigation using a mixed signal analog/digital neuromorphic processing system. *Front. Neurorobot.* **11**, 28 (2017).
14. J. L. Krichmar, Neurorobotics—A thriving community and a promising pathway toward intelligent cognitive robots. *Front. Neurorobot.* **12**, 42 (2018).
15. T. Matsui, H. Hirukawa, Y. Ishikawa, N. Yamasaki, S. Kagami, F. Kanehiro, H. Saito, T. Inamura, Distributed real-time processing for humanoid robots, in *11th IEEE International Conference on Embedded and Real-Time Computing Systems and Applications* (RTCSA, 2005), pp. 205–210.
16. T. C. Stewart, A. Kleinhans, A. Mundy, J. Conradt, Serendipitous offline learning in a neuromorphic robot. *Front. Neurorobot.* **10**, 1 (2016).
17. J. Conradt, F. Galluppi, T. C. Stewart, Trainable sensorimotor mapping in a neuromorphic robot. *Robot. Auton. Syst.* **71**, 60–68 (2015).
18. J. Pei, L. Deng, S. Song, M. Zhao, Y. Zhang, S. Wu, G. Wang, Z. Zou, Z. Wu, W. He, F. Chen, N. Deng, S. Wu, Y. Wang, Y. Wu, Z. Yang, C. Ma, G. Li, W. Han, H. Li, H. Wu, R. Zhao, Y. Xie, L. Shi, Towards artificial general intelligence with hybrid Tianjic chip architecture. *Nature* **572**, 106–111 (2019).
19. T. F. Nygaard, C. P. Martin, J. Torresen, K. Glette, D. Howard, Real-world embodied AI through a morphologically adaptive quadruped robot. *Nat. Mach. Intell.* **3**, 410–419 (2021).
20. D. Marković, A. Mizrahi, D. Querlioz, J. Grollier, Physics for neuromorphic computing. *Nat. Rev. Phys.* **2**, 499–510 (2020).
21. V. Braitenberg, Intricacies of movement control: An essay, in *Brain Theory: Spatio-Temporal Aspects of Brain Function*, A. Aertsen, Ed. (Elsevier, 1993), pp. 119–126.
22. R. Pfeifer, J. Bongard, S. Grand, *How the Body Shapes the Way We Think: A New View of Intelligence* (MIT Press, 2007).
23. B. Chen, H. Yang, B. Song, D. Meng, X. Yan, Y. Li, Y. Wang, P. Hu, T.-H. Ou, M. Barnell, Q. Wu, H. Wang, W. Wu, A memristor-based hybrid analog-digital computing platform for mobile robotics. *Sci. Robot.* **5**, eabb6938 (2020).
24. C. Wang, Z. Yang, S. Wang, P. Wang, C.-Y. Wang, C. Pan, B. Cheng, S.-J. Liang, F. Miao, A Braitenberg vehicle based on memristive neuromorphic circuits. *Adv. Intell. Sys.* **2**, 1900103 (2020).
25. R. A. John, N. Tiwari, M. I. B. Patdillah, M. R. Kulkarni, N. Tiwari, J. Basu, S. K. Bose, Ankit, C. J. Yu, A. Nirmal, S. K. Vishwanath, C. Bartolozzi, A. Basu, N. Mathews, Self healable neuromorphic memtransistor elements for decentralized sensory signal processing in robotics. *Nat. Commun.* **11**, 4030 (2020).
26. P. Gkoupidenis, N. Schaefer, B. Garlan, G. G. Malliaras, Neuromorphic functions in PEDOT:PSS organic electrochemical transistors. *Adv. Mater.* **27**, 7176–7180 (2015).
27. P. Gkoupidenis, N. Schaefer, X. Strakosas, J. A. Fairfield, G. G. Malliaras, Synaptic plasticity functions in an organic electrochemical transistor. *Appl. Phys. Lett.* **107**, 263302 (2015).
28. W. Xu, S.-Y. Min, H. Hwang, T.-W. Lee, Organic core-sheath nanowire artificial synapses with femtojoule energy consumption. *Sci. Adv.* **2**, e1501326 (2016).
29. Y. van de Burgt, E. Lubberman, E. J. Fuller, S. T. Keene, G. C. Faria, S. Agarwal, M. J. Marinella, A. A. Talin, A. Salleo, A non-volatile organic electrochemical device as a low-voltage artificial synapse for neuromorphic computing. *Nat. Mater.* **16**, 414–418 (2017).
30. A. Melianas, T. J. Quill, G. LeCroy, Y. Tuchman, H. V. Loo, S. T. Keene, A. Giovannitti, H. R. Lee, I. P. Maria, I. McCulloch, A. Salleo, Temperature-resilient solid-state organic artificial synapses for neuromorphic computing. *Sci. Adv.* **6**, eabb2958 (2020).
31. Y. Kim, A. Chortos, W. Xu, Y. Liu, J. Y. Oh, D. Son, J. Kang, A. M. Foudeh, C. Zhu, Y. Lee, S. Niu, J. Liu, R. Pfattner, Z. Bao, T.-W. Lee, A bioinspired flexible organic artificial afferent nerve. *Science* **360**, 998–1003 (2018).
32. G. Malliaras, R. Friend, An organic electronics primer. *Phys. Today* **58**, 53–58 (2005).

33. T. Someya, Z. Bao, G. G. Malliaras, The rise of plastic bioelectronics. *Nature* **540**, 379–385 (2016).
34. B. D. Paulsen, K. Tybrandt, E. Stavrinidou, J. Rivnay, Organic mixed ionic–electronic conductors. *Nat. Mater.* **19**, 13–26 (2020).
35. S. T. Keene, C. Lubrano, S. Kazemzadeh, A. Melianas, Y. Tuchman, G. Polino, P. Scognamiglio, L. Cinà, A. Salleo, Y. van de Burgt, F. Santoro, A biohybrid synapse with neurotransmitter-mediated plasticity. *Nat. Mater.* **19**, 969–973 (2020).
36. E. J. Fuller, S. T. Keene, A. Melianas, Z. Wang, S. Agarwal, Y. Li, Y. Tuchman, D. James, M. J. Marinella, J. J. Yang, A. Salleo, A. A. Talin, Parallel programming of an ionic floating-gate memory array for scalable neuromorphic computing. *Science* **364**, 570–574 (2019).
37. J. Hawkins, Special report : Can we copy the brain? - What intelligent machines need to learn from the Neocortex. *IEEE Spectr.* **54**, 34–71 (2017).
38. M. Gasperi, P. Hurbain, *Extreme NXT: Extending the Lego Mindstorms NXT to the Next Level* (Apress, 2009).
39. J. Rivnay, S. Inal, A. Salleo, R. M. Owens, M. Berggren, G. G. Malliaras, Organic electrochemical transistors. *Nat. Rev. Mater.* **3**, 17086 (2018).
40. K. H. Lee, M. S. Kang, S. Zhang, Y. Gu, T. P. Lodge, D. C. Frisbie, "Cut and stick" rubbery ion gels as high capacitance gate dielectrics. *Adv. Mater.* **24**, 4457–4462 (2012).
41. A. Giovannitti, D.-T. Sbircea, S. Inal, C. B. Nielsen, E. Bandiello, D. A. Hanifi, M. Sessolo, G. G. Malliaras, I. McCulloch, J. Rivnay, Controlling the mode of operation of organic transistors through side-chain engineering. *Proc. Natl. Acad. Sci. U.S.A.* **113**, 12017–12022 (2016).
42. D. A. Bernards, G. G. Malliaras, Steady-state and transient behavior of organic electrochemical transistors. *Adv. Funct. Mater.* **17**, 3538–3544 (2007).
43. S. Inal, G. G. Malliaras, J. Rivnay, Benchmarking organic mixed conductors for transistors. *Nat. Commun.* **8**, 1767 (2017).

Acknowledgments: We acknowledge F. Keller, A. Steinmetz, and A. Becker from the Max Planck Institute for Polymer Research (MPIP) for significant contribution in the design and realization of the experimental setup (maze, 3D-printed parts, and video recording) and electronics (customization of the robot and additional hardware for conditioning). We also acknowledge H.-J. Guttmann and C. Bauer for assistance in the clean room facilities of MPIP. We also acknowledge G. Malliaras for relevant preliminary discussions and B. Meijer for support. **Funding:** Facilities of MPIP (clean room, device metrology, electronics, and mechanical workshop) are supported by the Max Planck Society (to P.W.M.B. and P.G.). nano@Stanford laboratories are supported by the National Science Foundation as part of the National Nanotechnology Coordinated Infrastructure under award ECCS-1542152 (to A.S.). This study is funded by a joint project between MPIP and the Institute for Complex Molecular Systems (ICMS), Eindhoven University of Technology, grant no. MPIPICMS2019001 (to Y.v.d.B., I.K., and P.G.); European Union's Horizon 2020 Research and Innovation Programme, grant agreement no. 802615 (to Y.v.d.B.); the Carl-Zeiss Foundation (to P.G.); National Science Foundation and the Semiconductor Research Corporation, E2CDA award no. 1739795 (to A.S. and S.T.K.); and Stanford Graduate Fellowship fund (to S.T.K.). **Author contributions:** I.K., Y.v.d.B., A.S., and P.G. conceived the project and designed the experiments. A.M., I.K., S.T.K., D.A.K., A.G., Y.v.d.B., A.S., and P.G. investigated materials and tuned their properties. I.K., D.A.K., K.L., S.T.K., A.M., and P.G. designed, fabricated, and characterized the devices and the neuromorphic circuit. I.K., H.L., and P.G. designed and implemented the maze, the robot, electronics, and control algorithms. R.S., A.G., and I.M. designed, synthesized, and provided the semiconducting material(s). P.G. and F.T. performed the simulations and the circuit modeling. I.K., Y.v.d.B., A.S., and P.G. prepared the manuscript with input from all the authors. Y.v.d.B., P.G., and P.W.M.B. acquired the financial support. **Competing interests:** The authors declare that they have no competing interests. **Data and materials availability:** All data needed to evaluate the conclusions in the paper are present in the paper and/or the Supplementary Materials. LEGO MINDSTORMS is a trademark and copyright of the LEGO Group.

Submitted 18 July 2021
Accepted 22 October 2021
Published 10 December 2021
10.1126/sciadv.abl5068